Regional carbon fluxes and the effect of topography on the variability of atmospheric CO2.

van der Molen, M.K.; Dolman, A.J.

published in
Journal of Geophysical Research. Atmospheres
2007

DOI (link to publisher)
10.1029/2006JD007649

document version
Publisher's PDF, also known as Version of record

Regional carbon fluxes and the effect of topography on the variability of atmospheric CO_2

M. K. van der Molen[1] and A. J. Dolman[1]

Received 14 June 2006; revised 6 September 2006; accepted 26 September 2006; published 12 January 2007.

[1] Using a mesoscale atmospheric circulation model, it is shown that relatively modest topography height differences of ~500 m over 200 km near Zotino (60°N, 89°E) in central Siberia may generate horizontal gradients in CO_2 concentration in the order of 30 ppm. In a case study for 15 and 16 July 1996, when Lloyd et al. (2001) conducted a convective boundary layer budget experiment in the area, we show that advection of these gradients disturbs the relation between diurnal concentration changes in the boundary layer and the surface fluxes. This demonstrates that mesoscale atmospheric heterogeneity may have severe impact on the applicability of methods to derive the regional-scale fluxes from CO_2 concentrations measurements, such as the convective boundary layer budget method or inverse modeling. It is shown that similar mesoscale gradients are likely to occur at many long-term observation stations and tall towers. We use the modeled concentration fields to quantify the horizontal and vertical variability of carbon dioxide in the atmosphere. In future observation campaigns, mesoscale processes may be best accounted for by measuring horizontal variability over a few hundred kilometers and by attempting to quantify the representation errors as a function of mesoscale conditions.

Citation: van der Molen, M. K., and A. J. Dolman (2007), Regional carbon fluxes and the effect of topography on the variability of atmospheric CO_2, *J. Geophys. Res.*, *112*, D01104, doi:10.1029/2006JD007649.

1. Introduction

[2] The rising concentration of atmospheric carbon dioxide in the atmosphere is cause for considerable concern since it causes substantial additional greenhouse warming. Anthropogenic emissions are the prime reason for the current increases in CO_2 concentration [*Prentice et al.*, 2001]. From the carbon dioxide emitted by fossil fuel combustion and deforestation and associated biomass burning only about 40% ends up in the atmosphere [*Houghton et al.*, 2001]. The ratio of the atmospheric increase versus fossil fuel emissions has remained remarkably constant since the first direct observations of CO_2 were started at Mauna Loa. To balance the budget, the remaining part must have been taken up by the land surface and the oceans [*Bousquet et al.*, 1999; *Rödenbeck et al.*, 2003]. The precise geographical distribution of the sinks on the land and ocean surface is still a matter of considerable controversy and depends largely on the availability of data, that are necessary in model inversions [e.g., *Rödenbeck et al.*, 2003]. It is important to understand the processes controlling the uptake of carbon dioxide by the surface, so that the exchange rate and variability can be predicted under the influence of climatic change. From the perspective of the Kyoto protocol and UNFCC convention, Annex 1 countries are required to map source and sink distributions on a regional (national/state) scale, because anthropogenic emissions may be partially balanced by natural sinks. Therefore there is an increasing demand for methods to derive regional CO_2 fluxes.

[3] There are several meteorological based methods that may be used to assess the surface fluxes of carbon dioxide, each with its own characteristic spatial and temporal coverage. We discuss three commonly used methods. The first, eddy covariance, uses the concentration difference between up and down moving eddies to calculate the surface flux [*Valentini et al.*, 2000a; *Reichstein et al.*, 2002; *Wilson et al.*, 2002a, 2002b, 2003; *Janssens et al.*, 2003; *Dolman et al.*, 2003; *Ciais et al.*, 2005]. The method typically provides continuous data on a half-hourly basis, that are representative for a footprint in the order of hundreds of meters. Eddy covariance data are useful to study the processes of photosynthesis and respiration [cf. *Dolman et al.*, 2004a]. The limited footprint is a disadvantage when one wants to measure the average flux over a larger, heterogeneous region. The problem may be overcome by installing eddy towers in a large number of typical ecosystems such as is done by FLUXNET [*Baldocchi et al.*, 2001], EUROFLUX [*Aubinet et al.*, 2000; *Valentini et al.*, 2000a] and TCOS-Siberia [*Heimann*, 2002].

[4] The second method, the convective boundary layer (CBL) budget method, takes advantage of the generally well mixed properties of the CBL, in which changes in the carbon dioxide concentration profile reflect the surface fluxes [*Lloyd et al.*, 2001; *Styles et al.*, 2002; *Laubach and Fritsch*, 2002; *Betts et al.*, 2004; *Cleugh et al.*, 2004;

[1]Department of Hydrology and Geo-Environmental Sciences, Faculty of Earth and Life Sciences, Vrije Universiteit Amsterdam, Amsterdam, Netherlands.

0148-0227/07/2006JD007649

Schmitgen et al., 2004]. The CBL budget method provides flux data that are representative at a spatial scale in the order of the height of the CBL. The CBL budget method is therefore useful for estimating the average surface fluxes of landscapes that are heterogeneous on a smaller scale, so that the effect of changing surface fluxes is blended. This scale lies between what is commonly called the local and regional scale and is effectively of the order of kilometers. The time resolution is usually a few hours, and the duration of CBL budget experiments is often one day. Experiments may be repeated a few successive days. The applicability of the convective boundary layer budget method is limited under the following conditions: (1) when the quasi-Lagrangian approach is violated and advection plays a role [*Lloyd et al.*, 2001; *Laubach and Fritsch*, 2002; *Styles et al.*, 2002; *Cleugh et al.*, 2004; *Schmitgen et al.*, 2004]; (2) when the entrainment flux (i.e., the flux that results from thermals overshooting the top of the boundary layer and thereby incorporating air from the free atmosphere into the boundary layer) is large with respect to the surface fluxes, the requirements on instrumental accuracy become high [*Lloyd et al.*, 2001]; (3) when boundary layer mixing is not sufficient, various layers may be advected in the CBL [*Schumacher*, 2005]; (4) when the subsidence (the downward air velocity that occurs above the boundary layer in high-pressure areas) strength is unknown or variable; (5) when the boundary layer height is variable under influence of topography or a heterogeneous surface heat or momentum flux distribution; and (6) when the CBL column moves over a heterogeneous surface it is hard to assess the compare the results with eddy covariance data collected at a fixed location. In practice CBL budget experiments are designed such that the effect of these limitations are expected to be small by selecting appropriate weather conditions and/or by estimating the associated errors. Although satisfactory results are regularly obtained [e.g., *Lloyd et al.*, 2001], it is not always understood why the method sometimes works better than at other times. The majority of the limitations listed above may be collected under the name "3-D representation errors" and they typically occur on a scale that is resolved in mesoscale atmospheric models.

[5] The third, the inverse modeling method, combines large-scale concentration gradients with atmospheric transport to determine source/sink regions. This method was initially used to infer surface fluxes on continental/ocean basin scales [*Bousquet et al.*, 1999; *Gurney et al.*, 2002; *Rödenbeck et al.*, 2003], but in recent years there is a tendency to investigate the possibility of regional-scale inversions [*Gerbig et al.*, 2003a, 2003b; *Dolman et al.*, 2005, 2006; R. J. Ronda et al., The potential of an Eularian inverse transport approach for deriving the regional distribution of surface fluxes of carbon dioxide from measured concentrations at a tall tower, manuscript in preparation, 2006]. Because the atmospheric circulation integrates the effects of source/sink distributions when the air moves over the continent, the temporal resolution of the fluxes is in the order of days. Synoptic-scale atmospheric mixing is a main driving process. However, in practice monthly mean gradients are often used in inversions, reducing the time resolution accordingly. The inverse modeling methods are limited by four types of errors [*Denning et al.*, 1996; *Gurney et al.* ; *Gerbig et al.*, 2003a, 2003b; *Rödenbeck et al.*, 2003; *Lin and Gerbig*, 2005]: representation errors, aggregation errors, rectification errors and transport model errors. Of these the representation error, that arises from the mismatch between a point observation and a grid cell average, is addressed in this study.

[6] Next to these meteorological approaches, forest inventories and crop biomass accounting may provide long-term (seasonal to interannual) constraints to the surface fluxes of carbon on limited spatial scales. Each of the above methods thus provides flux estimates at well-defined spatial and temporal scales. There is not a single best method to obtain flux data with global coverage at a high resolution, so that a combination of methods may be needed to do so [*Dolman et al.*, 2005, 2006]. One scale, the mesoscale, is not well represented in the methods presented above. Mesoscale processes are typically related to heterogeneity in the order of 10 to 100 km, somewhat larger than addressed by the CBL budget method, but smaller than addressed by the (regional) inverse models. Examples of mesoscale processes are sea (forest, river) breezes, urban heat islands and topographically induced circulations [cf. *Pielke and Uliasz*, 1998; *Pielke et al.*, 1999; *Dolman et al.*, 2004b; *van der Molen et al.*, 2006] and they may result in air circulations and convergence. Other mesoscale circulations are caused by variability in cloud cover (radiation) and soil moisture [*Chan et al.*, 2004]. In the following it will be shown that many limitations of the CBL budget method and the inverse modeling method are related to mesoscale processes.

[7] It is the objective of this paper to demonstrate the use of mesoscale models to quantify some of the most important of these errors. We explore how the "3-D representation error" in the CBL budget method may be estimated and we attempt to quantify the representation error of point measurements of CO_2 concentration and its relation to spatial resolution, that is important to the inverse modeling methods. We discuss the implications of mesoscale variability on the methods to derive regional-scale CO_2 fluxes and show that many CO_2 measuring stations around the world may be subject to mesoscale processes.

2. Methods

2.1. Model Description

[8] The mesoscale model was set up around Zotino in central Siberia (60°N, 89°E). Long time series of eddy flux measurements and profile measurements have been taken in the area [*Schulze et al.*, 1999; *Lloyd et al.*, 2001; *Shibistova et al.*, 2002; *Styles et al.*, 2002; *Tchebakova et al.*, 2002], making it a relevant study area. Moreover, Siberian forests constitute 60% of the boreal forests and 20% of the global forest area and they are considered modulators of the global climate [*Bonan et al.*, 1992; *Pielke and Uliasz*, 1998] and net sinks of CO_2 [*Tans et al.*, 1990; *Gurney et al.*, 2002; *Rödenbeck et al.*, 2003]. An additional advantage of a case study in central Siberia is that anthropogenic emissions are negligible. The location near Zotino and the dates, 15 and 16 July 1996, are chosen for this study to match those when *Lloyd et al.* [2001] applied the CBL budget method to derive the average flux over a landscape mosaic of forest and bogs. They obtained three profiles per day up to between 2000 and 3000 m using an aircraft, in the morning,

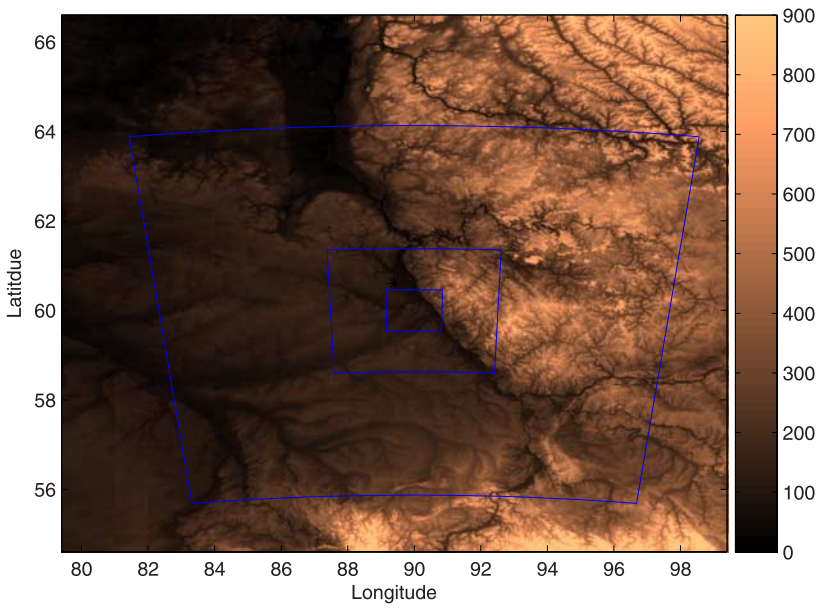

Figure 1. Topographical map of the research area with height in meters. The boxes indicate the domains of the parent grid plus the two nested grids. The location of the flux tower is in the northwestern corner of the finest grid.

midday and evening. Because of an unexpected change in wind direction during the experiment, they were not completely able to follow the air mass in a Lagrangian way, so that advection may have influenced the observed profiles. The entrainment flux was relatively large compared to the surface flux, which reduced the accuracy of the derived fluxes.

[9] We use the Regional Atmospheric Modeling System (RAMS) [*Pielke et al.*, 1992, 1999] to simulate the effects of turbulent mixing, advection and cloud condensation on the atmospheric fields of wind, temperature, water vapor and CO_2 using a finite differences scheme and a terrain following coordinate system. The surface boundary conditions are represented by the General Energy Mass Transfer Model (GEMTM) [*Chen and Coughenour*, 1994, 2004], that takes into account the effects of stomatal control on the surface fluxes of heat, water and CO_2 for 30 different plant functional types. Initial and boundary conditions are prescribed using the European Center for Medium-Range Weather Forecasts (ECMWF) reanalysis data (http://www.ecmwf.int/research/era/) to include the large-scale gradients in air pressure, wind speed, air temperature and humidity. The subsidence velocity is thus directly related to the convergence/divergence of the wind field. The CO_2 concentration is initialized homogeneously at 360 ppm. Topography heights are taken from the global United States Geological Survey (USGS) topography data set (30 arcsec or about 1 km, http://bridge.atmet.org/users/data.php). The *Chen and Cotton* [1983] radiation scheme for short- and long-wave radiation is employed. The domain consists of 32×35 grid cells each spanning 27 km, thus covering 864×945 km^2. The surface is represented by evergreen needleleaf trees. In the vertical the domain extends to a height of 14 km with a layer thickness of 30 m near the surface, which increases with a factor of 1.15 toward the top, but with a maxi hickness of 1250 m. Nested within this coarse domain are two grids with increasingly finer horizontal resolutions of 9 and 3 km, but the same number of grid cells. The domains of the three grids are shown in the topographical map of Figure 1. The model is run for 42 hours from 15 July 1996 0600 local standard time (LST) (= UTC − 8) until 17 July 0000 LST with time steps of 120 s on the coarse grid.

[10] We used RAMS with only standard options for vegetation class and soil type and easily accessible topography data and atmospheric fields from the European Centre for Medium-Range Weather Forecasts (http://www.ecmwf.int) reanalyses. We did not calibrate the vegetation model to obtain correct surface fluxes and we did not implement heterogeneous vegetation cover. This had the advantage that the approach was simple and easily applicable for other locations and that the physics behind the results are more easily understood. Obviously, this bears the danger of misrepresenting the surface fluxes and not being able to simulate precisely all the air circulations arising from contrasting vegetation types, e.g., forest-bog, forest-pasture transitions [*Baidya Roy et al.*, 2003; *Dolman et al.*, 2004b]. However, by artificially introducing a checkerboard pattern of heterogeneity in the surface fluxes of CO_2 and/or stomatal conductance, we show that such mesoscale circulations do not have much effect in the current situation.

2.2. Artificial Checkerboard Heterogeneity

[11] For two reasons a checkerboard pattern in the surface fluxes is artificially introduced in the model: (1) to create a signal in the CO_2 concentration field, that can be used to analyze the horizontal and vertical mixing efficiency, and (2) to observe whether variations in the Bowen ratio (the ratio of the sensible over the latent heat flux) may initiate mesoscale circulations. The heterogeneity is forced upon the fluxes in one of the two following ways: (1) by halving the net surface CO_2 flux simulated by the vegetation model and

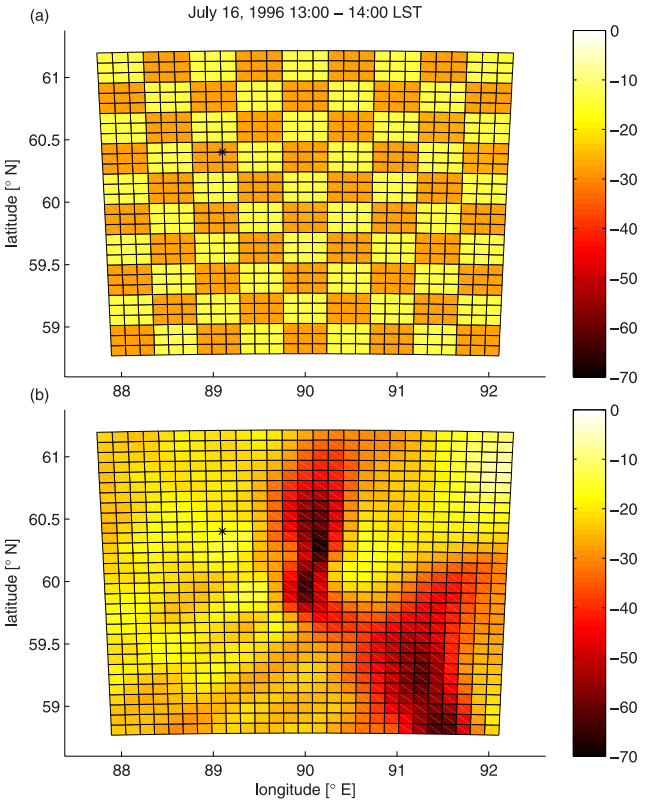

Figure 2. (a) Simulated surface fluxes f_{sfc} (equation (1)) compared with (b) the simulated change in column content of CO_2 f_{CBL} (equation (2)) between 1300 and 1400 LST on day 2 (16 July 1996) expressed in μmol m^{-2} s^{-1}. Results are shown for the middle grid with a grid size of 9 × 9 km^2 and checkerboard fields of 27 × 27 km^2. The cross mark indicates the location of the flux tower.

(2) by increasing the stomatal resistance 10-fold, which results in an increase of the Bowen ratio from about 0.3 to 0.75. The first way introduces a CO_2 concentration signal that is not correlated to temperature or moisture, whereas the second way introduces a concentration signal that is correlated to buoyancy, so that the CO_2 signal may possibly be transported by mesoscale disturbances. The manipulation is applied to a subset of all surface grid cells in a checkerboard pattern, with field sizes that were changed from 3 × 3 km^2 to 6 × 6 km^2, 9 × 9 km^2, 18 × 18 km^2 and 27 × 27 km^2. Thus, in the finest grid, with a resolution of 3 × 3 km^2, the fields span 1 × 1, 2 × 2, 3 × 3, 6 × 6 or 9 × 9 cells, respectively. In the middle grid, with a resolution of 9 × 9 km^2, the checkerboard fields are not resolved when the size is 3 × 3 km^2 or 6 × 6 km^2. In the coarsest grids the checkerboard fields are not resolved at all (because the finer grids are staggered with respect to the coarser grids). We use the results of the simulations with a heterogeneity of the first type (only CO_2 fluxes are modified, not stomatal resistance) and a field size of 27 × 27 km^2, unless explicitly stated otherwise.

2.3. Description of Area and Weather Conditions

[12] The area around Zotino in central Siberia is covered by a rather homogeneous land cover mosaic of Scots Pine (Pinus *sylvestrus*) and *S um* bogs with a typical length scale of a kilometer, which is subgrid-scale in the current model setup [*Wirth et al.*, 1999; *Valentini et al.*, 2000b; *Lloyd et al.*, 2001]. This land cover is typical for the west Siberian lowlands between the Ural Mountains and the Yenisey river, where there is little relief and the terrain elevation is around 200 m. The Yenisey river forms the western boundary of the east Siberian plains, with a maximum elevation of about 700 m at about 100 km east of the river (Figure 1). The slope between the east Siberian plains and the Yenisey river is thus relatively modest. The east Siberian plains slope downward toward the Lena River in the east and are covered predominantly by Larix spp. NDVI (Normalized Difference Vegetation Index) and vegetation cover maps are presented by *Lloyd et al.* [2001].

[13] The weather conditions on [*Lloyd et al.*, 2001, p. 274] "the two experimental days were characterized by mild and mostly clear sky conditions with maximum air temperatures at the base camp of 20° and 26°C for July 15 and 16, respectively. The only cloud observed during the 2-day period was a patchy fair weather cumulus cloud of limited depth around midday on July 15." A high-pressure area was moving eastward over the area, causing a shift in wind direction from north to east in the night between 15 and 16 July, and further clearing to southeast during the day, whereas wind speeds in the boundary layer decrease from 5 to 10 m s^{-1} on the first day to below 5 m s^{-1} on the second day. Ground level pressure maps are shown in *Lloyd et al.* [2001] at 12 hour intervals during the campaign.

3. Results

3.1. Evaluation of the CBL Budget Method

[14] The applicability of the CBL budget method is assessed by comparing the surface CO_2 flux of each grid cell with the change of the carbon dioxide content in the corresponding column. Figure 2a shows the temporal mean surface flux (f_{sfc}) of carbon dioxide, calculated as:

$$f_{sfc}(i,j) = \frac{1}{T}\int_{T} NEE(i,j)\,\partial t \qquad (1)$$

where *NEE* is the net ecosystem exchange, the difference between respiration and assimilation as simulated by the vegetation module in RAMS, T is the averaging time, which is from 1300 to 1400 LST on 16 July, the second day of the simulation, i and j are the indices to the longitude and latitude of the grid cells. The *NEE* is output from the vegetation module in RAMS and is a function of solar radiation, temperature, humidity, soil moisture, wind speed, etc. In this simulation the *NEE* was reduced to 50% for certain cells following a checkerboard pattern with the field size 27 × 27 km^2 (see section 2.2). The results for the medium grid are shown here. Figure 2b shows the change in the content of carbon dioxide in the atmospheric columns overlying the corresponding grid cells from 1300 to 1400 LST:

$$f_{CBL}(i,j) = \frac{1}{M_{CO_2} T}\int_{z=0}^{z_{max}} \rho_{CO_2}(i,j,k)\partial z \qquad (2)$$

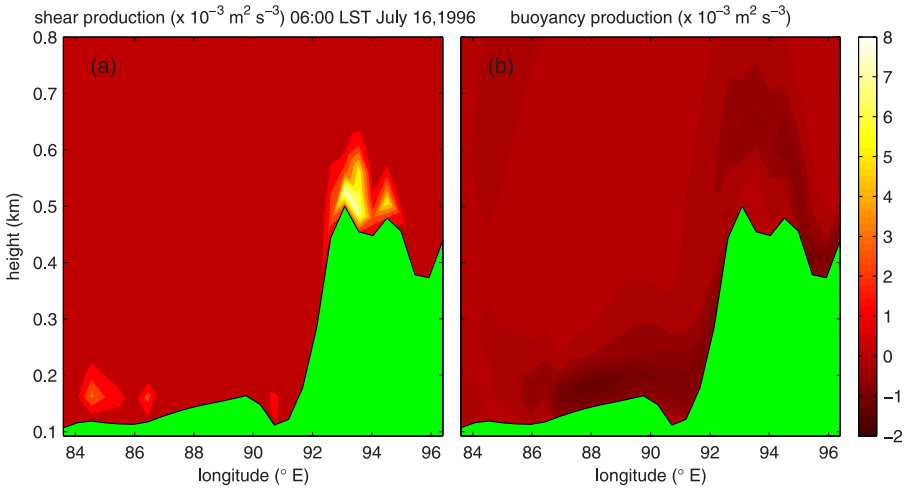

Figure 3. Production of turbulent kinetic energy by (a) wind shear and (b) buoyancy in the morning (0600 LST) of the second day of the simulation. All contours in Figure 3b are negative, indicating consumption of TKE by buoyancy. The cross sections are drawn at 59.2°N.

where M_{CO2} = 44.01 g mol^{-1}, ρ_{CO2}(i, j, k) the carbon dioxide density of each grid cell and z_{max} some height well above the CBL, where ρ_{CO2} is constant in time and height. f_{CBL} represents the carbon dioxide surface flux that would be derived when the CBL budget method is applied to the simulated CO_2 concentration profiles in each column (we use "CO_2 concentration" as a synonym of "CO_2 mixing ratio"). Because the profiles extend to high above the boundary layer, the effects of entrainment and subsidence are implicitly accounted for, but advection is neglected. When advection and horizontal diffusion between grid cells are indeed negligible, and no other sources or sinks are present, $f_{sfc}(i, j)$ must equal $f_{CBL}(i, j)$. In the western part of the domain (Figure 2b) the effect of surface flux heterogeneity may be recognized to a certain extent in the change in atmospheric content, but in the central and eastern part of the domain, f_{CBL} is very different from f_{sfc}, which shows that advection can indeed not be neglected. Here a band of high f_{CBL} may be seen, implying that a CBL budget experiment conducted in that area would estimate surface fluxes that are very different from the actual surface fluxes.

3.2. Explanation of the Mismatch Between f_{sfc} and f_{CBL}: Effect of Topography

[15] The formation of the band of high f_{CBL} is closely related to the development and nonuniform breakup of the nocturnal boundary layer, as explained in the next paragraphs. During the night carbon dioxide accumulates in the nocturnal boundary layer (NBL). The NBL is shallow, ~200 m deep and stable, so that the CO_2 concentrations are >40 ppm higher than in the residual layer above. However, turbulent mixing intensity is not constant throughout the domain, because a local maximum occurs on the edge of the east Siberian plateau and a local minimum in the valley below. This is demonstrated in Figure 3, which shows the patterns of production of turbulent kinetic energy due to (1) wind shear and (2) buoyancy at 0600 LST on 16 July 1996, in a cross section through the domain. In this instance the shear production is nonnegative in the entire domain and particularly pronounced at the plateau's edge, whereas the buoyancy production is negative in the entire domain, meaning that turbulence is consumed, with the strongest consumption in the lower parts of the domain. The minimum in turbulence intensity in the valley leads to a particularly shallow NBL and subsequently high concentrations of respired CO_2. Drainage of cold air may be another reason for the low concentrations on the plateau's slope.

[16] This pattern of turbulence intensity is conform to the theory described by *Kaimal and Finnigan* [1994], who show that under moderately stable conditions the mean wind speed has a maximum above hill tops and decreases on lee slopes. In a similar way, the momentum flux near the surface has a maximum above hill tops, of about two times the undisturbed magnitude ($f_{uw,0}$). Halfway down the lee slopes the momentum flux decreases to about 0.5 × $f_{uw,0}$, from where it slowly returns to its normal value. At higher levels the momentum flux behaves almost oppositely, it has a minimum of 0.5 × $f_{uw,0}$ above the hill top and increases 1.5 to 2.5 × $f_{uw,0}$. The impact of a hill on the atmospheric flow may extend to tens of hill heights down wind (~10 km in this situation).

[17] Figure 3 shows the patterns of turbulence production at 0600 LST because the contrast between edge and valley is most pronounced at this time just before sunrise. After sunrise solar heating of the surface causes a rather homogeneous buoyancy production in the entire domain, but the maximum of shear production above the hill top is maintained. The contrast between mixing intensity above the top and in the valley and the higher CO_2 concentration in the NBL in the valley causes a strong horizontal CO_2 concentration gradient, illustrated by Figure 4a, which is valid at 1000 LST. The solid line indicates the boundary layer height, defined as the lowest height where the turbulent kinetic energy is smaller than 5 × 10^{-4} m^2 s^{-2}. At this time it becomes evident that the boundary layer is deeper toward the west of the domain, in comparison to the relative minimum above the valley, which is the reason why the CO_2 concentrations remain highest over the valley. 1000 LST is the time when the horizontal concentration

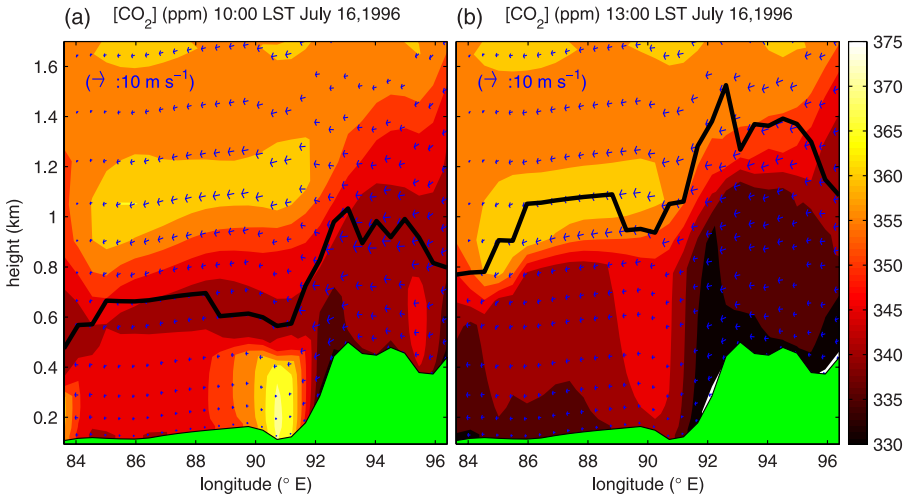

Figure 4. Cross section of the simulated CO_2 concentration field of the coarsest grid at (a) 1000 LST and (b) 1300 LST on 16 July 1996. The contours indicate concentration differences at 5 ppm intervals and the solid line represents the boundary layer height. The arrows indicate longitudinal and vertical ($\times 20$) wind velocity, and a scale indication is shown in the top left. The surface topography is also shown. Note that the horizontal extent of the domain covers 864 km, so that the horizontal is much more compressed relative to the vertical. The cross sections are drawn at 59.2°N.

gradient is most pronounced, although it does not lead to strong distortion of the f_{CBL} yet, because the wind speed in the CBL is small. Later in the day, around midday, the wind speed increases in the CBL, possibly as a result of better coupling of the CBL to the free atmosphere. At about 1300 LST the westward transportation of the concentration gradients by the mean wind results in the band of high f_{CBL} in Figure 2b, resembling high surface uptake. Thus this band is caused by advection of CO_2 concentration gradients. Figure 4b illustrates that the location of the high f_{CBL} band occurs where the concentration gradient is largest (~91°E), which corresponds to the rear side of the air mass of high CO_2 concentration. In that area the CO_2 content of the atmospheric column decreases with time and to the CBL budget method this resembles an area of strong surface uptake of CO_2. On the front side of the air mass with higher concentrations the concentration gradients are not as strong as on the back side, which is why the corresponding area of low f_{CBL} is hardly visible.

3.3. Verification That the CO_2 Concentration Gradients Are Caused by Topography

[18] We corroborated these results with two simulations where the topography height was respectively reduced to 50% (Figure 5a) and 0% of its original value (Figure 5b). In these simulations the concentration gradients at the location of the slope disappeared partially and completely, respectively, which indicates that the concentration gradients discussed above are indeed caused by the variability in turbulence production along the sloping topography. However, a different concentration gradient is observed, most clearly in Figure 5b, at the eastern edge of the domain. This

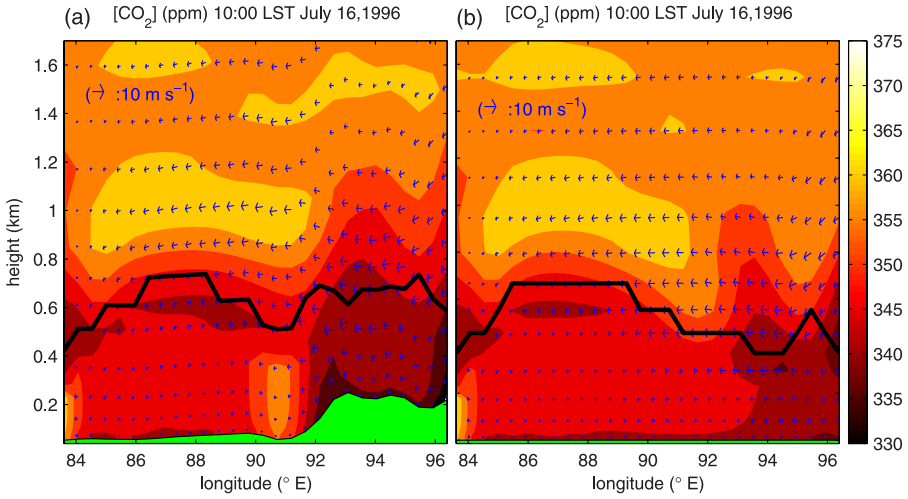

Figure 5. (a and b) Same as Figure 4 but with the topography reduced to 50% and 0% of the value in Figure 4.

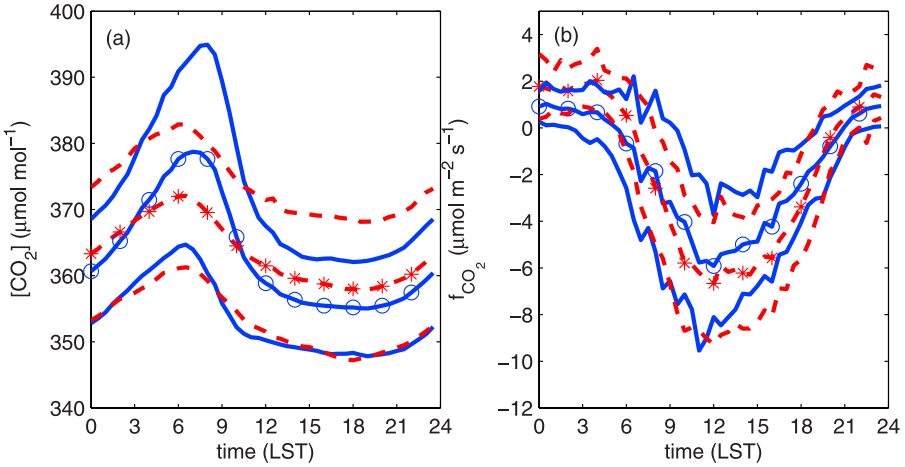

Figure 6. Average diurnal cycles of CO_2 (a) concentration and (b) flux under conditions of easterly winds (solid lines with open circles) and westerly winds (dashed lines with asterisks). The corresponding lines without markers indicate ±1 standard deviation. The data represent half hourly averages collected at the Zotino forest eddy flux tower from day of year 150 until 250 in the years 1998 to 2003. The clustering of wind direction is based on the mean wind direction between 0430 and 1630 LST.

is a boundary artifact and arises from an overnight shift in the wind direction from outflow to inflow, under influence of the synoptic-scale pressure gradient. At the inflow boundaries, a zero-gradient boundary condition is maintained for CO_2, so that the concentration of the inflowing air is kept at the low concentrations of the early night residual layer. If anything, this demonstrates the need to put the lateral (and top) boundaries far away from the area of interest. Figure 5b also shows substantial variations in boundary layer height in the absence of topography. This is the result of the variable divergence and convergence of the wind field as a function of the pressure gradients of the overpassing high-pressure cell and the resulting subsidence velocity [*Lloyd et al.*, 2001, Figure 1]. However, there are no concentration gradients associated with this variability in the boundary layer height, most likely because the subsidence velocity does not correlate with the surface or entrainment fluxes.

3.4. Verification of Model Results With Flux Tower Data

[19] We use data from the Zotino forest flux tower, the location of which is marked by the cross in Figure 2a, to investigate whether the explanation of section 3.2 is realistic. Figure 6a shows the average diurnal cycles of CO_2 concentration during the summer period, between day of year 150 to 250 (29 May to 6 September), in the years 1998 until 2003, separately for conditions with easterly and westerly winds. With easterly winds, the average morning peak concentration is significantly higher than in westerly winds, suggesting that the simulated advection of air with high CO_2 concentrations is a common phenomenon in this region. Figure 6b shows that the surface CO_2 flux does not change with wind direction. In addition, Figure 7 shows that the time of peak is earlier with increasing easterly wind, but not for westerly winds, which suggests that advection is indeed the responsible process. However, Figures 6 and 7 do not explain why the CO_2 concentration is higher during easterly winds. This co ve alternative reasons, such as a different sink/source strength of the east Siberian plains with respect to the west Siberian lowlands.

3.5. Verification of the Model Results With Profile Data

[20] The simulated temperature profiles and the inversion height closely matched the observations made from the aircraft (not shown). The shapes of the CO_2 concentration profiles were in fairly good agreement with the observed profiles [*Lloyd et al.*, 2001, Figure 3], but the concentration changes in time were not correct on the second day of the experiment. Remarkably, on that day, 16 July 1996, the observed profiles showed a light increase in CBL CO_2 concentration during the day (344 ppm in the morning, 347 ppm in the afternoon and 349 ppm in the evening), whereas our simulations showed a decrease (∼340 ppm in the morning and afternoon, 335 ppm in the evening, Figure 8). *Lloyd et al.* [2001] explain the increasing concentration with the large entrainment flux relative to the surface flux, which would "overcompensate" the surface flux. Consequently, we explain the difference between simulated and observed profiles by the larger simulated surface fluxes (max ~ -22 μmol m^{-2} s^{-1} averaged over the checkerboard fields) compared to the observed ones (max ~ -9 μmol m^{-2} s^{-1} [*Lloyd et al.*, 2001, Figure 12]). As a result, the ratio of entrainment flux to surface flux was smaller in our simulations. This explanation was tested by performing a simulation where the simulated surface fluxes were reduced to better match the observed surface fluxes (see Table 1). As a first guess, the average surface fluxes were reduced by assigning all grid cells the fluxes of the low checkerboard fields, so that they were about -15 μmol m^{-2} s^{-1} in the entire domain at noon of the second day. Figure 9 shows the corresponding CO_2 concentration profiles, together with the flask concentration measurements redrawn after [*Lloyd et al.*, 2001]. On the first day, the simulated profiles do not yet show the structure of the observed profiles, but the evening profiles match well. In the morning of the second day the simulated

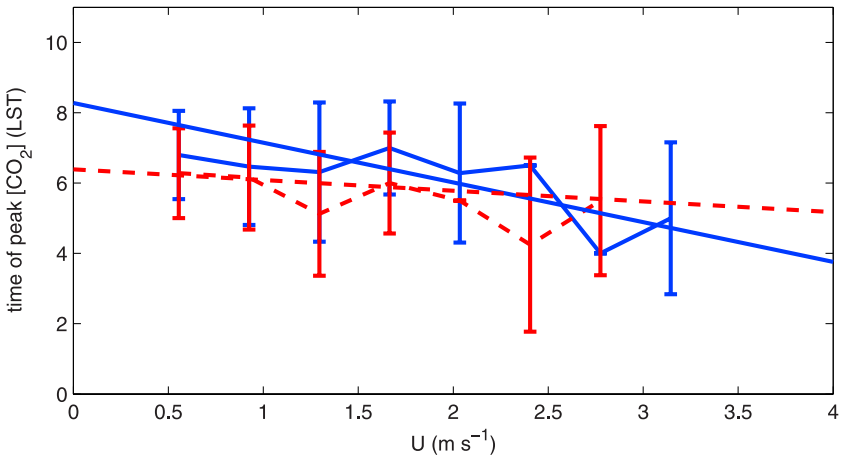

Figure 7. Time of peak CO_2 concentration as function of the average morning wind speed under conditions of easterly wind directions (solid line) and westerly wind directions (dashed line). The straight lines represent the least squares linear regression lines. The data represent half hourly averages collected at the Zotino forest eddy flux tower from day of year 150 until 250 in the years 1998 to 2003. The clustering of wind direction is based on the mean wind direction between 0430 and 1630 LST.

residual boundary layer is a bit too shallow, indicating problems of modeling the stable boundary layer, but during the day it grows toward the observed values. The CBL CO_2 concentrations on the second day are now 348 ppm in the morning, 349 ppm in the afternoon and 347 ppm in the evening, which is indeed closer to the observations. Thus the high uptake rate in the uncalibrated standard model may explain the difference between modeled and observed CO_2 profiles in the afternoon of 16 July 1996. Although the simulated and observed concentrations do not match exactly, the reasonably well simulated shape of the profiles and the inversion height, as well as the sensitivity to the surface fluxes give confidence that the model sufficiently describes the dynamics in the CBL.

[21] Another reason why the CO_2 concentration may have increased in the afternoon of 16 July 1996 is the arrival of

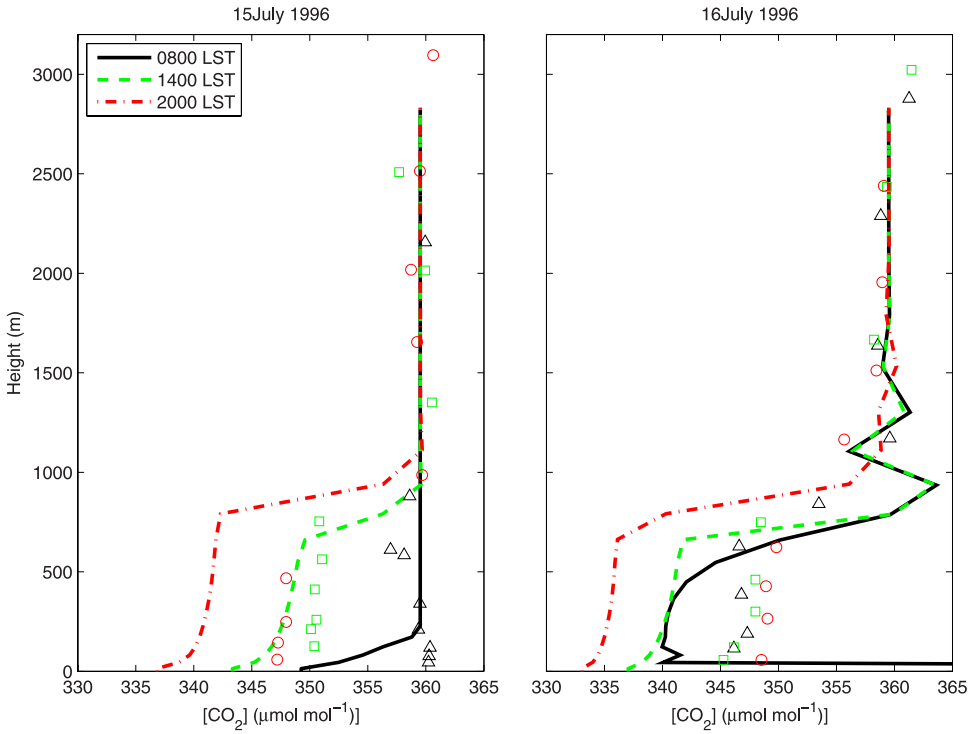

Figure 8. Simulated profiles of CO_2 concentration at the time and at the location closest to where *Lloyd et al.* [2001] performed observations. These profiles are obtained from the standard simulation with checkerboard pattern surface fluxes, where the surface CO_2 uptake is overestimated. The triangles, squares and circles indicate the observed carbon dioxide concentrations using flasks at 0800 LST, 1330 LST and 1930 respectively (redrawn after *Lloyd et al.* [2001]).

Table 1. A Rough Estimation of the Change of the Boundary Layer Concentration as a Function of the Surface Flux in the Afternoon[a]

		Normal Fluxes		Reduced Fluxes	
Variable	Units	15 July	16 July	15 July	16 July
$[CO_2]$ 1400 LST	ppm	348	340	352	350
$[CO_2]$ 2000 LST	ppm	341	335	348	347
d $[CO_2]$	ppm	−7	−5	−4	−3
f_{co2}	μmol m^{-2} s^{-1}	−19.5	−16.5	−12.2	−9.25
$d[CO_2]/f_{co2}$	ppm/μmol m^{-2} s^{-1}	0.36	0.30	0.33	0.32

[a]$d[CO_2]$ indicates the change in CO_2 concentration between 1400 and 2000 LST, and f_{CO2} refers to the surface flux of CO_2. $d[CO_2]/f_{co2}$ indicates the change in boundary layer concentration per unit flux.

the air mass of higher CO_2 concentration. The locations where the profile measurements are performed are indicated by the asterisks labeled 4 to 6 in Figure 10 and are located in the area of high concentrations, just west of the band of the apparently high surface uptake, which was caused by advection of the CO_2 gradient.

[22] The arguments in the sections 3.3 to 3.5 give direct and indirect evidence to support the model results. More precise verification could be obtained by measuring horizontal CO_2 concentration gradients and variations in the height of the boundary layer. However, these measurements were not made. Maybe more importantly, the observers probably would not have known to collect those data, without performing such model simulations. The modeling results so far show that small variations in topography may cause organized CO_2 gradients in the CBL that do not reflect patterns in the surface fluxes.

3.6. Quantification of the Representation Error

[23] In sections 3.1 to 3.5 it has been shown that 3-D variability in turbulent mixing imposes serious limitations on the CBL budget method, and that mesoscale atmospheric circulation models may be used to estimate the effect on the observed profiles. As discussed in the introduction, one of the major issues in inverse modeling is the spatial representativeness of point observations of CO_2 concentration. Our simulations may be used to estimate the representation error as a function of distance from the location of the point measurements. In order to do so, we defined 16 virtual measurement locations in a 4 × 4 matrix with an internal distance of 7 grid spacings. Next, we expressed the representation error of the measurements as the standard deviation of the CO_2 concentration in a circular field with radius r around the 16 locations and by varying the radius. Thus small radii resemble a fine resolution of the observation network or a fine resolution of the transport model in inversion. In this way, the representation error is similar to the one presented by *Gerbig et al.* [2003a, Figure 5], except that theirs also includes the measuring inaccuracy. Figure 11 shows the average standard deviation of these 16 fields for 3 height levels, one near the surface at 47 m, one within the CBL at 296 m and one above the boundary layer at 1545 m, as represented by different line style-color

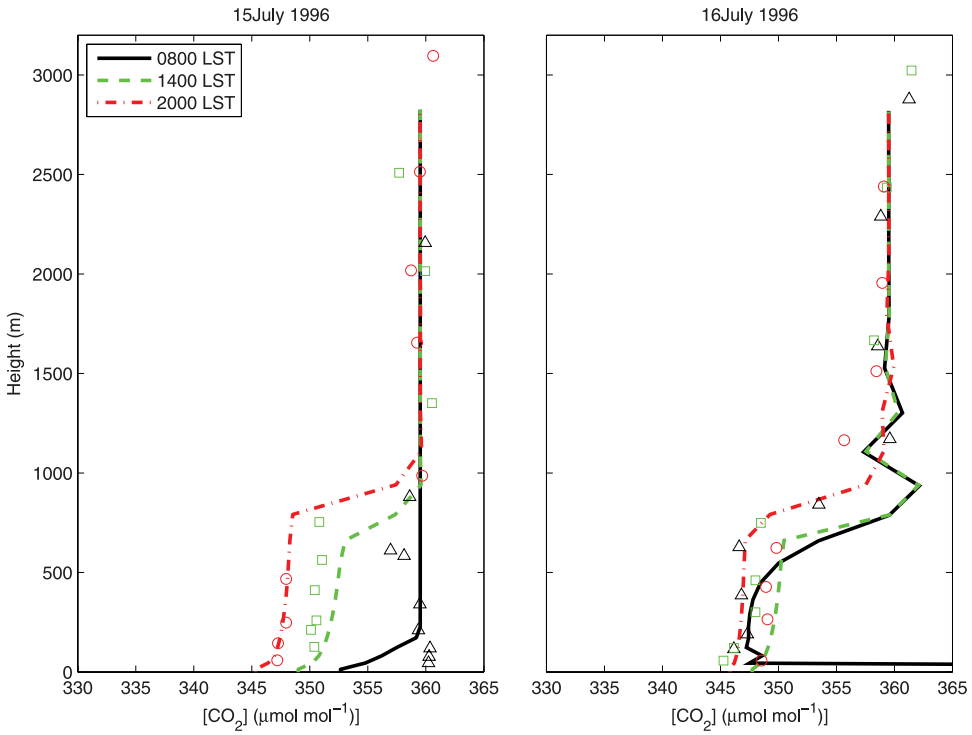

Figure 9. Simulated profiles of CO_2 concentration at the time and at the location closest to where *Lloyd et al.* [2001] performed observations. These profiles are obtained from a simulation, where the surface CO_2 uptake is reduced by about 33% with respect to the standard stimulation in order to better match the surface fluxes observed by the eddy covariance system [*Lloyd et al.*, 2001]. The triangles, squares and circles indicate the observed carbon dioxide concentrations using flasks at 0800 LST, 1330 LST and 1930 LS ectively (redrawn after *Lloyd et al.* [2001]).

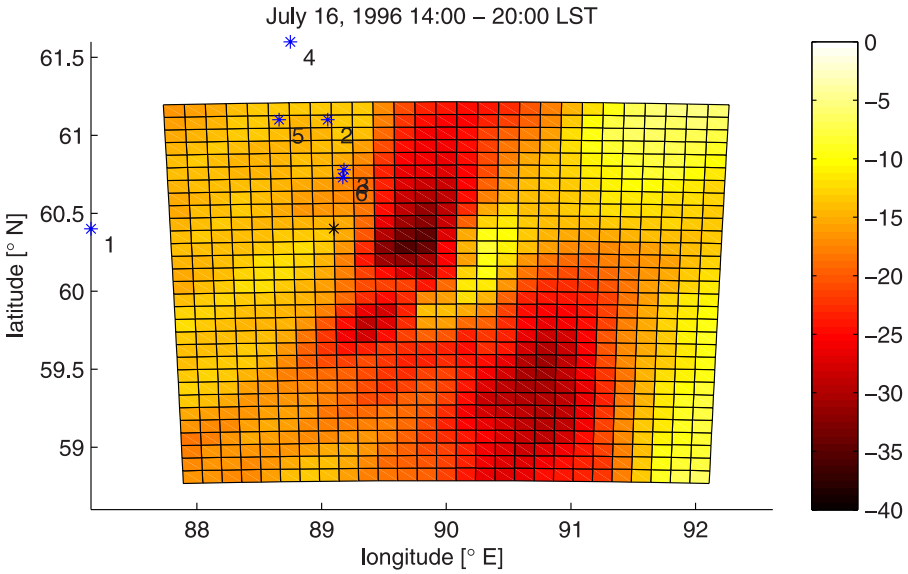

Figure 10. Change in total column carbon dioxide content on 16 July 1996 between 1400 and 2000 LST expressed as a surface flux in μmol m^{-2} s^{-1}. The asterisks represent the locations where profile observations 1–6 by *Lloyd et al.* [2001] are taken.

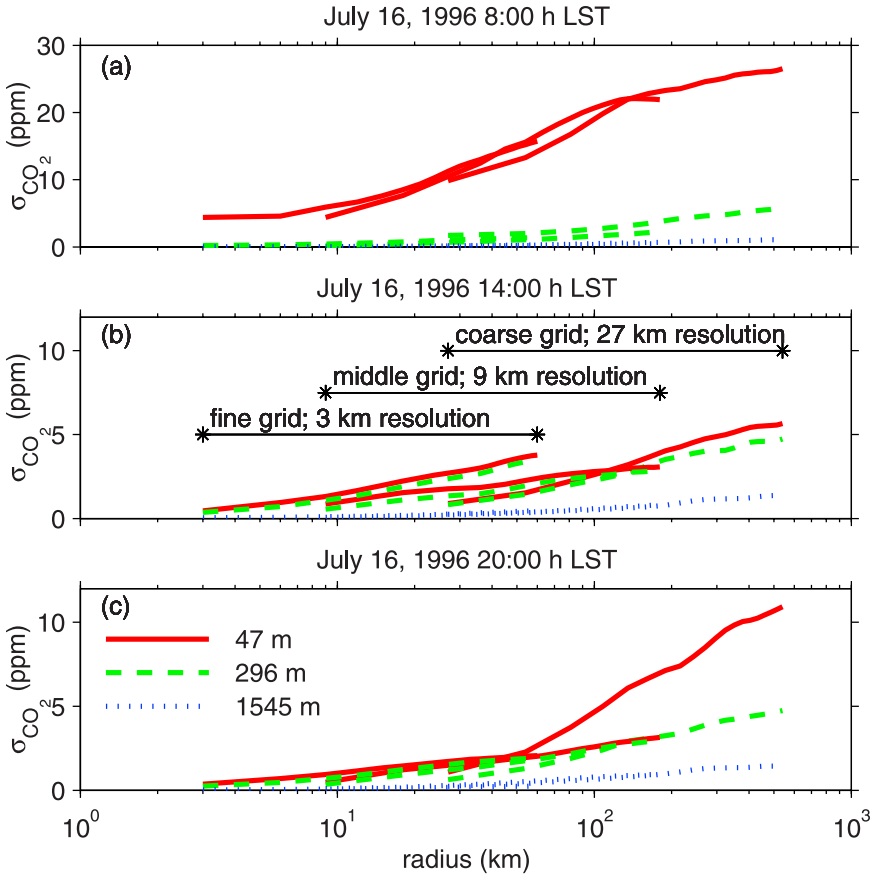

Figure 11. Representation error as a function of the distance, expressed as the standard deviation (y axis) of the CO_2 field in a circle with a varying radius (x axis) at (a) 0800 LT, (b) 1400 LT, and (c) 2000 LT. The solid lines indicate the representation error at 47 m above the ground, the dashed lines represent the error at 296 m and the dotted lines indicate the error at 1545 m. The overlapping lines of identical style indicate t resentation error of the fine, middle and coarse grid.

combinations. Figures 11a, 11b, and 11c represent the results at 0800, 1400 and 2000 LST, respectively, according to the time of the profiles taken in *Lloyd et al.* [2001]. The representation error for a single time and height is shown for three overlapping ranges of radii, representing the results of the fine, medium and coarse model grid.

[24] Figure 11a shows that in the morning carbon dioxide concentrations collected near the ground had a representation error of about 5 ppm for radii smaller than the size of the checkerboard fields (27 km). The representation error increased to more than 20 ppm at distances longer than 100 km. At higher levels the grid cell concentrations were representative within 1 ppm until ~30 km at the 296 m level and until ~500 km at the 1545 m level. Figure 11b shows that the representation error of the 47 m level was much smaller at 1400 LST under influence of the convective mixing. The 47 and 296 m level agreed well at that time and the 1 ppm representation error was already reached at a radius of about 10 km and at the 1545 m level at about 200 km. At a radius of 30 km, the coarse grid consistently had smaller representation errors than the middle and fine grids. This is because the checkerboard surface flux pattern is not resolved in the coarse grid. The results suggest that increasing the resolution below 10–20 km added little more to the reduction of the representation error at midday. Figure 11c indicates that at 2000 LST the 1 ppm representation error at 1545 m was reached again at a somewhat shorter distance, ~150 km. In the lower levels not much changed with respect to earlier in the day, except that the error at the 47 m level increased sharply beyond a radius of ~50 km, suggesting that the surface was already decoupling and that variations at the scale of the topography differences had the strongest impact. Coarser resolution domains typically had a lower error at the same radius, indicating that information was lost by aggregating grid cells. However, this picture was somewhat obscured because coarser grids also have larger domains, which could give rise to extra variability.

[25] In these simulations, the checkerboard pattern caused a variability in the CO_2 concentration, which was passively mixed into the CBL. In reality, CO_2 flux variability is often coupled to heterogeneity in the Bowen ratio, so that turbulence generated by buoyancy differences may spread the CO_2 signal actively into the CBL. This may be considered to be a spatial form of the rectifier effect, after *Denning et al.* [1996] who used the term "rectifier effect" to indicate the temporal (diurnal/seasonal) covariance between CO2 flux and turbulent mixing efficiency. To investigate if such a spatial rectifier effect should be expected in the current experimental conditions, a simulation was performed where variations in the carbon dioxide fluxes in the checkerboard were associated with variations in the Bowen ratio. The Bowen ratio was varied 0.35 and 0.75 in the fields with low and high CO_2 fluxes, respectively (it was about 0.3 in the standard setup). In these simulations, the representation error did not change significantly in the morning and at midday, but it clearly increased at 2000 LST, for the fine grid, in the boundary layer and for radii from 6 to 30 km, where the error increased in the order of 0.5–1 ppm (from 1.0 to 1.5 ppm at 10 km and from 2.1 to 2.8 ppm at 27 km). This suggests that small-scale forest-bog breezes may develop in the area if a clear contrast in Bowen ratio exists between various landsc mponents, thus introducing a covariance between turbulence transport and CO_2 concentration. This experiment also shows that the representation error is a function of surface energy and carbon dioxide flux heterogeneity and that it may also be influenced by weather conditions, which may determine the strength and size of the forest-bog circulation. The turbulence intensity may also change with vegetation type because of changes in surface roughness, but this effect was not simulated. This simplification is probably allowed because under the light wind conditions, the contrast in buoyancy with land cover heterogeneity dominates over the contrast in wind shear.

[26] Figure 11 may be used to decide how far the resolution of atmospheric circulation models should be increased to yield a significant reduction in the representation error. It is seen that coarser grids have larger representation errors, but they also have the largest gain with enhanced resolution. In the CBL the representation error typically decreases with 2.5 ppm with a 10 times increased resolution in the CBL. In the free troposphere this is typically 0.5 ppm and it is in the order of 10 ppm in the NBL. The change becomes smaller when moving toward lower grid spacings, indicated by the concave shape of the lines in Figure 11, suggesting that saturation occurs at some resolution below 10 km. At all levels with exception of the NBL, the representation error increases during the day. Above the boundary layer the representation errors are much smaller, although there appears to be a diurnal cycle, where in the afternoon the error increases faster with distance than in the morning. This may be caused by variations in turbulence intensity in the boundary layer, which cause variations in the boundary layer height and distortions in the flow pattern in the air above the boundary layer.

3.7. Change in Representativeness With Height

[27] A related issue is how the representativeness of a carbon dioxide observation changes with height in the boundary layer and to what height surface heterogeneity influences the atmospheric concentrations. This matter is important in order to determine at what height concentration measurements need to be taken. Using the simulated atmospheric fields, Figure 12 shows the correlation coefficient (r^2) between the carbon dioxide concentration at the surface and at height z, normalized by the boundary layer height. The correlation is determined by the influence of the checkerboard pattern of high and low fluxes on the carbon dioxide concentration of the overlying air, as well as by mesoscale variations in turbulent mixing intensity (see Figure 2). The correlation coefficient is large in the lower layers and decreases with height because of turbulent diffusion in the horizontal and vertical directions and because of advection. Figure 12 shows that in the course of the day, the atmospheric CO_2 concentrations become better linked to the surface. From midday onward, $r^2 > 0.8$ in the lower half of the mixed layer and r^2 decreases sharply to below 0.25 at higher levels. The correlation coefficients are larger for the fine and medium grids than for the coarse grid and this may be related to the scale of the variability in CO_2 concentration with regard to the resolution of the respective grid. In this case the checkerboard pattern of surface fluxes and the topography are major causes of variability. Because the checkerboard fields are not resolved

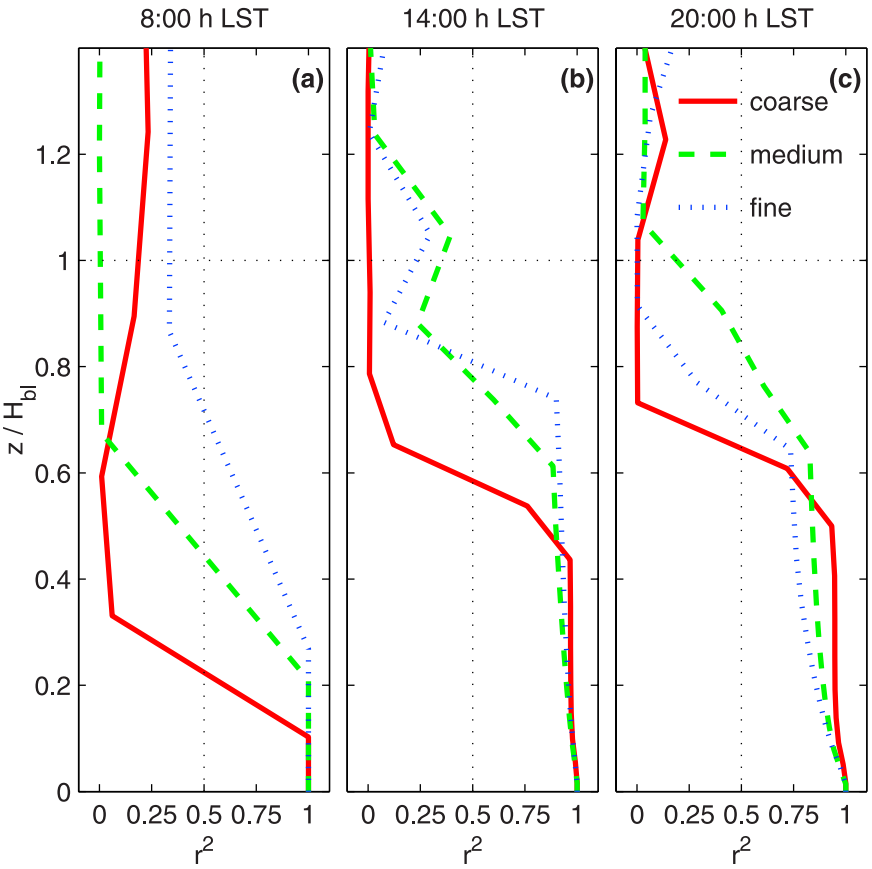

Figure 12. Correlation between the carbon dioxide concentrations at the surface and at height z (scaled with the boundary layer height, H_{bl}) at (a) 0800, (b) 1400 and (c) 2000 LST. The r^2 for the coarse, medium and fine grid are indicated by the solid line, dashed line and the dotted line, respectively. The model results for 16 July 1996 are used, with a checkerboard field size of 27 × 27 km^2.

in the coarse grid, the correlation coefficient is determined solely by mesoscale variability in the carbon dioxide concentrations. The causes of this mesoscale variability have been discussed in sections 3.1 and 3.2, and Figure 12 reconfirms their importance. However, variability on the scale of the checkerboard patterns adds considerably to the correlation coefficient for the finer grids. The correlations are not much different in the case where the carbon flux variability was coupled to the Bowen ratio, nor when the size of the checkerboard fields is changed. Figure 12 suggests that the effect of surface heterogeneity is best observed in the lower part of the boundary layer. In this case, the lower part extends to about halfway up the boundary layer, but it is unknown if this is generally valid. Above that height, the signal of surface heterogeneity is much smaller, which implies that concentration changes result from surface fluxes in a much larger footprint. This suggest that the concept of blending height may also be applicable to CO_2. The blending height is a scale that indicates at which height above the surface the atmospheric profiles are blended so that the effect of surface flux heterogeneity may not be distinguished. Below the blending height, the atmosphere is not homogeneous and the profiles are strongly related to the respective surface fluxes [*Wieringa*, 1986; *Dolman and Blyth*, 1996]. However, because the correlation coefficient decreases gradually, there is no level that is particularly suitable to measure the effect of the averaged fluxes of a fixed region. It would be interesting if figures such as Figure 12 could be made for other studies, preferably with verifying observations, and if relations could be made with topography, vegetation cover or stability regime.

3.8. Topographical Situation Around Zotino Compared With Other Stations

[28] Finally, Table 2 shows a list of locations where CBL budget experiments were conducted, of stations with tall towers and a selection of long-term carbon dioxide concentration observatories. The selection includes many of the stations that are frequently used in CO_2 inversions, but with the exception of most of the stations located on islands. Of the 32 stations in the list, 17 are 100 km or less from the coast, implying that they could be regularly under the influence of sea breezes, which is among the strongest prototypes of mesoscale circulations. Note that the Baltic Sea station is located offshore. Table 2 also indicates the height of the stations as well as the 10- and 90-percentile topography heights in the segments located to the north, east, south and west of the stations. These segments extend to 200 km from the station, roughly coinciding with the distance over which the concentration gradients in Figures 2 and 4 appear during the day. The maximum topography height difference, dz_{max}, was defined as the maximum over

Table 2. A Selection of Sites Where CBL Budget Experiments Were Conducted, Sites With Tall Towers and Long-Term CO_2 Concentration Monitoring Sites, With Their Distance to the Coast, the Height of the Station, and the 10- and 90-Percentile of Heights in the North, East, South and West Segments Extending 200 km From the Station[a]

Station	Country	Latitude	Longitude	Distance to Coast, km	Height ASL, m	Heights Per Segment, m								dz_{max}, m
						p_{10}	p_{90}	p_{10}	p_{90}	p_{10}	p_{90}	p_{10}	p_{90}	
CBL Budget Experiments [Lloyd et al., 2001; Styles et al., 2002; Laubach and Fritsch, 2002; Schmitgen et al., 2004, Cleugh et al., 2004]														
Zotino	Russian Federation	60°36′	89°24′	>200	160	61	257	94	478	101	181	116	178	318
Hainich	Germany	51°6′	10°24′	>200	430	39	324	71	587	259	505	85	444	391
Le Bray	France	44°42′	0°46′	200	61	85	422	195	982	109	457	12	119	921
Wagga Central	Australia	−35°4′	147°20′	>200	212	251	374	304	1127	180	1012	104	179	915
Tall Towers (http://www.cmdl.noaa.gov/ccgg/towers.html, http://www.chiotto.org)														
Bialowieza	Poland (330 m)	52°15′	22°45′	>200	160	122	181	138	188	152	253	91	193	93
Cabauw	Netherlands (200 m)	51°58′	4°56′	38	−0.7	−4	−1	1	94	8	280	−1	19	280.7
Florence	Italy (245 m)	43°49′	11°16′	100	178	5	391	25	892	52	503	30	1036	858
Griffin	Great Britain (232 m)	56°33′	−2°59′	20	340	58	489	3	156	52	404	67	579	337
Grifton	NC, USA (610 m)	35°22′	−77°24′	80	9	6	104	1	9	4	19	24	152	143
Hegyhatsal	Hungary (117 m)	46°57′	16°39′	>200	248	117	497	92	246	102	292	256	1308	1060
Moody	TX, USA (505 m)	31°19′	−97°20′	>200	239	136	334	70	152	91	308	294	518	279
Norunda	Sweden (102 m)	60°5′	17°28′	49	45	11	245	3	37	1	59	38	324	279
Ochsenkopf	Germany (177 m)	50°3′	11°49′	>200	1193	90	476	220	724	363	520	251	518	1103
Orleans	France (203 m)	46°58′	2°7′	>200	390	88	180	170	494	270	848	61	200	458
Park Falls	WI, USA (447 m)	45°57′	−90°16′	>200	472	183	485	243	513	290	457	259	442	289
Tsukuba	Japan (200 m)	36°4′	140°7′	43	25	68	1019	1	33	3	200	29	1467	1442
Selected Sites From the WMO World Data Centre for Greenhouse Gasses (ttp://gaw.kishou.go.jp/wdcgg.html)														
Alert	Canada	82°27′	62°31′	0	210	...	...	13	261	26	379	8	347	210
Baltic Sea	Poland	55°21′	17°13′	67	28	4	99	7	157	26	180	4	141	152
Barrow	Alaska, USA	71°19′	156°35′	1	11	1	1	1	60	8	112	13	60	101
Black Sea	Romania	44°10′	28°40′	0	3	1	139	1	12	25	283	10	278	280
Law Dome	Antarctica (Australia)	−66°44′	112°50′	100	1390	167	1250	139	1215	704	1595	317	1547	1251
Mace Head	Ireland	53°19′	−9°54′	0	25	6	256	48	172	38	303	1	25	278
Mauna Loa	Hawaii, USA	19°32′	−155°34′	39	3397	89	2252	61	1943	107	2920	117	2477	3336
Monte Cimone	Italy	44°11′	10°42′	60	2165	11	885	4	694	15	518	68	977	2161
Mould Bay	Canada	76°15′	−119°20′	1	58	3	81	2	333	2	153	1	136	275
Pallas	Finland	67°58′	24°7′	>200	565	310	526	162	340	86	235	218	710	479
Palmer Station	Antarctica (USA)	−64°55′	−64°0′	0	10	65	810	57	1586	161	1750	8	803	1740
Plateau Assy	Kazakhstan	43°15′	77°52′	>200	2519	460	1533	538	3398	1601	4126	508	3252	2059
Schauinsland	Germany	47°55′	7°55′	>200	1205	117	480	394	1611	445	2422	225	811	1217
South Pole	Antarctica (USA)	−88°2′	−24°48′	>200	2810	2249	2441	2358	2723	2597	2762	2211	2712	599
Summit	Greenland (Denmark)	72°34′	−38°28′	>200	3238	2897	3146	2781	3133	3023	3083	2809	3078	457
Syowa Station	Antarctica (Japan)	−69°0′	39°35′	0	29	...	...	732	1875	410	1413	162	1409	1846

[a]All heights are taken from the USGS GTOPO30 data with a resolution of 30 arcsec or about 1 km (http://edc.usgs.gov/products/elevation/gtopo30/gtopo30.html), except the height A.S.L., which represents the actual base height. The height of the tall towers is given between brackets following the country name.

the four segments of $dz_{max} = (z_{station} - p_{10})$ and $(p_{90} - z_{station})$, where $z_{station}$ is the height of the station. Subsequently dz_{max} was grouped into the classes $dz_{max} < 250$ m, $250 < dz_{max} < 500$ m and $dz_{max} > 500$ m. For example, for Zotino $dz_{max} = 384$ m, occurring in the east segment. There are only 5 stations in the first class, 13 stations in the second class and 14 stations in the third class. These numbers indicate that the majority of the selected stations (27) have topography differences in the same range (250–500 m) or larger as Zotino in at least one of the segments, which means significant mesoscale flows affecting the CBL structure can be expected at their locations.

4. Discussion and Conclusions

[29] The convective boundary layer budget and the inverse modeling methods use the temporal changes in atmospheric CO_2 concentration to infer carbon dioxide surface fluxes. The limitations of those methods are often related to mesoscale three dimensional variability [*Laubach and Fritsch*, 2002; *Cleu h et al.*, 2004; *Geels et al.*, 2004, 2006]. This study demonstrates how relatively modest relief may cause horizontal carbon dioxide concentration gradients of 35 ppm in the boundary layer that exist for hours. The advection of such gradients causes concentration changes in time which disturb the link between surface fluxes and atmospheric concentration changes. Other causes of mesoscale variability in the atmosphere include variations in turbulence intensity, Bowen ratio, surface roughness, boundary layer height, subsidence velocity and/or entrainment flux.

[30] It is surprising that such relatively modest height differences (of ~500 m over 200 km) may cause so large CO_2 concentration gradients, because topography effects on wind, temperature and moisture fields are generally confined to a smaller area. For example, sea breezes, among the strongest mesoscale phenomena, usually reach no more than 100 km inland [*Xian and Pielke*, 1991; *van der Molen et al.*, 2006]. This is probably because CO_2 is a long-lived, passive tracer.

[31] The CO_2 concentration gradient of 35 ppm is of similar strength as the mean diurnal cycle observed at the

flux tower (Figure 6a). Moreover, the effect of advection of this concentration gradient on the boundary layer concentrations is 3–6 times larger than the effect of the surface uptake (Figure 2). The representation errors of 1–5 ppm (Figure 11), which are partially related to mesoscale phenomena, are also large in comparison to the diurnal variation in boundary layer concentrations of 15 ppm on 15 July and 5 ppm on 16 July 1996 (Figure 9). The fact that such strong concentration gradients appear in the simulation and that the topography differences are relatively modest compared to the majority of the stations listed in Table 2, suggest that mesoscale variability may significantly influence many CO_2 observation stations around the world.

[32] The effect of mesoscale variability on CO_2 concentrations cannot be neglected when performing inverse modeling or CBL budget experiments. The question arises how these mesoscale phenomena should be dealt with. It would be tempting to suggest that a mesoscale model simulation should be performed for each concentration measurement that is collected or that the transport models used for inversions should have nested grids that zoom toward the measurement locations. However, considerations are that mesoscale model runs are much more time consuming than coarser models and that the analysis of the model results involves dealing with many factors. Many causes of mesoscale variability are related to land surface heterogeneities that change in time, such as land cover, soil moisture, cloudiness, etc., which would also need to be simulated correctly. Simulating the effect of topography is thus a relatively easy case. Moreover, observations of mesoscale variability are needed to constrain the models. Still, this study demonstrates that mesoscale processes may not generally be neglected.

[33] Thus there is a pressing need to both incorporate mesoscale processes in CBL budget experiments and inverse modeling studies and at the same time to reduce the complexity of doing so. We suggest that future experiments to derive the surface fluxes of carbon dioxide on a regional scale make more effort to observe the horizontal variability of carbon dioxide over a distance of a few hundred kilometers. The focus would, on the one hand, be on collecting the observations needed to verify the simulated gradients and, on the other hand, to collect data to verify the representation error of point measurements (Figure 11) as well as the vertical correlation coefficients (Figure 12) and to try and relate those variables to weather conditions, topography and land surface heterogeneity. If such relations may successfully explain mesoscale variability, then some sort of "mesoscale site characterization" [cf. *Nicholls et al.*, 2004] may be developed to reduce the complexity. It would also be very interesting to provide observational evidence that the CO_2 concentrations in the lower part of the boundary layer are much better correlated to land surface heterogeneity than in the upper part (Figure 12). Most ideally this would be performed by flying multiple aircraft in horizontal legs above each other. It is possible that the CO_2 concentration profiles are more complex in reality than in the simulations, which could make the conclusions on the basis of the related profiles of the correlation coefficient more subtle. Preliminary examples of such experiments in southwest France and Spain are given by *Dolman et al.* [2006] and *Perez-Land l.* [2006a, 2006b]. An alternative would be to use the model to select those conditions when mesoscale processes do not influence the CO_2 concentration observations. However, we would not recommend to use this method when deriving long-term surface fluxes, because the selected conditions may be biased with respect to general weather conditions.

[34] Another relevant subject is how far the resolution of mesoscale models should be refined to resolve the most important causes of variability. Our simulations indicated that the representation error was typically 5 ppm, 2.5 ppm and 1 ppm within the CBL at a distance of 500, 50 and 5 km, respectively, from the measurement location. Above the CBL they were much smaller but in the nocturnal boundary layer point measurements had representation errors of 5 to 25 ppm. The representation error typically decreases by 2.5 ppm with a 10-fold increase in resolution. More gain is obtained at coarse resolutions (>100 km) and less at small resolutions (<20 km). Using a variogram estimation of the representation error, *Gerbig et al.* [2003a] found that in models with a grid size >30 km the representation error dominates over the sampling inaccuracy, and it changes with the square root of the grid size, so that considerable improvement may be obtained by reducing the grid size below ~100 km. *Karstens et al.* [2006] suggest that measurement stations should optimally be distributed at a distance of a few hundreds of km. Our results seem to confirm these findings, but according to our results a further refinement of model grids may considerably reduce the errors associated to mesoscale processes. These results should also be compared with observations of the horizontal variability of the CO_2 concentration, and with model results for different locations and weather conditions. This may reveal the sensitivity of the representation error to environmental factors, and possibly to model setup.

[35] **Acknowledgments.** Olga Shebistova is gratefully acknowledged for making the eddy flux data available, and Reinder Ronda is acknowledged for his help in setting up RAMS for this study. The investigations were supported by the Research council for Earth and Life Sciences (ALW) with financial aid from the Netherlands Organization for Scientific Research (NWO, grant 854.00.018) and by the European Commission under the Fifth Framework Programme TCOS-Siberia (EVK2-2001-00143). Three reviewers are sincerely thanked for suggestions that improved the manuscript.

References

Aubinet, M., et al. (2000), Estimates of the annual net carbon and water exchange of forests: The EuroFlux methodology, *Adv. Ecol. Res.*, *30*, 113–176.

Baidya Roy, S., C. P. Weaver, D. S. Nolan, and R. Avissar (2003), A preferred scale for landscape forced mesoscale circulations?, *J. Geophys. Res.*, *108*(D22), 8854, doi:10.1029/2002JD003097.

Baldocchi, D. D., E. Falge, and L. H. Gu (2001), FLUXNET: A new tool to study the temporal and spatial variability of ecosystem-scale carbon dioxide, water vapor and energy flux densities, *Bull. Am. Meteorol. Soc.*, *82*, 2415–2434.

Betts, A. K., B. Helliker, and J. Berry (2004), Coupling between CO_2, water vapor, temperature, and radon and their fluxes in an idealized equilibrium boundary layer over land, *J. Geophys. Res.*, *109*, D18103, doi:10.1029/2003JD004420.

Bonan, G. B., D. Pollard, and S. L. Thomson (1992), Effect of boreal forest vegetation on global climate, *Nature*, *359*, 716–718.

Bousquet, P., P. Ciais, P. Peylin, M. Ramonet, and P. Monfray (1999), Inverse modeling of annual atmospheric CO_2 sources and sinks: 1. Methods and control inversion, *J. Geophys. Res.*, *104*(D21), 26,161–26,178.

Chan, D., C. W. Yuen, K. Higuchi, A. Shashkov, J. Liu, J. Chen, and D. Worthy (2004), On the CO_2 exchange between the atmosphere and the biosphere: The role of synoptic and meso-scale processes, *Tellus, Ser. B*, *56*(3), 194–212.

Chen, C., and W. R. Cotton (1983), A one-dimensional simulation of the stratocumulus capped mixed layer, *Boundary Layer Meteorol.*, *25*, 289–321.

Chen, D.-X., and M. B. Coughenour (1994), GEMTM: A general model for energy and mass transfer of land surfaces and its application at the FIFE sites, *Agric. For. Meteorol.*, *68*, 145–171.

Chen, D.-X., and M. B. Coughenour (2004), Photosynthesis, transpiration, and primary productivity: Scaling up from leaves to canopies and regions using process models and remotely sensed data, *Global Biogeochem. Cycles*, *18*, GB4033, doi:10.1029/2002GB001979.

Ciais, P., et al. (2005), Europe-wide reduction in primary productivity caused by the heat and drought in 2003, *Nature*, *437*, 533–539, doi:10.1038/nature03972.

Cleugh, H. A., M. R. Raupach, P. R. Briggs, and P. A. Coppin (2004), Regional-scale heat and water vapour fluxes in an agricultural landscape: An evaluation of CBL budget methods in OASIS, *Boundary Layer Meteorol.*, *110*, 99–137.

Denning, A. S., D. A. Randall, G. J. Collatz, and P. J. Sellers (1996), Simulations of terrestrial carbon metabolism and atmospheric CO_2 in a general circulation model. Part 2. Simulated CO_2 concentrations, *Tellus, Ser. B*, *48*, 543–567.

Dolman, A. J., and E. M. Blyth (1996), Patch scale aggregation of heterogeneous land surface cover for mesoscale meteorological models, *J. Hydrol.*, *190*, 252–268.

Dolman, A. J., E.-D. Schulze, and R. Valentini (2003), Analyzing carbon flux measurements, *Science*, *301*, 916–917.

Dolman, A. J., T. C. Maximov, E. J. Moors, A. P. Maximov, J. A. Elbers, A. V. Kononov, M. J. Waterloo, and M. K. van der Molen (2004a), Net ecosystem exchange of carbon dioxide and water of far eastern Siberian larch (*Larix dahurica*) on permafrost, *Biogeosciences*, *1*, 133–146.

Dolman, A. J., M. K. van der Molen, H. W. ter Maat, and R. W. A. Hutjes (2004b), The effect of forests on meso-scale atmospheric processes, in *Forests at the Land-Atmosphere Interface*, edited by M. Mencuccini et al., 304 pp., Oxford Univ. Press, New York.

Dolman, A. J., R. J. Ronda, F. Miglietta, and P. Ciais (2005), Regional measurement and modeling of carbon balances, in *The Carbon Balance of Forest Biomes*, edited by H. Griffiths and P. J. Jarvis, pp. 93–108, Taylor & Francis, Philadelphia, Pa.

Dolman, A. J., et al. (2006), CERES, the CarboEurope Regional Experiment Strategy in Les Landes, south west France, May–June 2005, *Bull. Am. Meteorol. Soc.*, *87*(10), 1367–1379.

Geels, C., S. C. Doney, R. Dargaville, J. Brandt, and J. H. Christensen (2004), Investigating the sources of synoptic variability in atmospheric CO_2 measurements over the Northern Hemisphere continents: A regional model study, *Tellus, Ser. B*, *56*, 35–50.

Geels, C., et al. (2006), Comparing atmospheric transport models for future regional inversions over Europe. Part 1: Mapping the CO_2 atmospheric signals, *Atmos. Chem. Phys. Disc.*, *6*, 3709–3756, sref:1680-7375/acpd/2006-6-3709.

Gerbig, C., J. C. Lin, B. C. Daube, A. E. Andrews, B. B. Stephens, P. S. Bakwin, and C. A. Grainger (2003a), Toward constraining regional-scale fluxes of CO_2 with atmospheric observations over a continent: 1. Observed spatial variability from airborne platforms, *J. Geophys. Res.*, *108*(D24), 4756, doi:10.1029/2002JD003018.

Gerbig, C., J. C. Lin, B. C. Daube, A. E. Andrews, B. B. Stephens, P. S. Bakwin, and C. A. Grainger (2003b), Toward constraining regional-scale fluxes of CO_2 with atmospheric observations over a continent: 2. Analysis of COBRA data using a receptor oriented framework, *J. Geophys. Res.*, *108*(D24), 4757, doi:10.1029/2003JD003770.

Gurney, K., et al. (2002), Towards robust regional estimates of CO_2 sources and sinks using atmospheric transport models, *Nature*, *415*, 626–630.

Heimann, M. (2002), The EUROSIBERIAN CARBONFLUX project, Foreword, *Tellus, Ser. B*, *54*, 417–419.

Houghton, J. T., Y. Ding, D. J. Griggs, M. Noguer, P. J. van der Winden, and X. Dai (Eds.) (2001), *Climate Change 2001: The Scientific Basis. Contribution of Working Group 1 to the Third Assessment Report*, 881 pp., Cambridge Univ. Press, New York.

Janssens, I. A., et al. (2003), Europe's terrestrial biosphere absorbs 7 to 12% of European anthropogenic CO_2 emissions, *Science*, *300*, 1538–1542, doi:10.1126/science.1083592.

Kaimal, J. C., and J. J. Finnigan (1994), *Atmospheric Boundary Layer Flows: Their Structure and Measurements*, 289 pp., Oxford Univ. Press, New York.

Karstens, U., M. Gloor, M. Heimann, and C. Rödenbeck (2006), Insights from simulations with high-resolution transport and process models on sampling of the atmosphere for constraining mid-latitude land carbon sinks, *J. Geophys. Res.*, *111*, D12301, doi:10.1029/2005JD006278.

Laubach, J., and H. Fritsch (2002), Convective boundary layer budgets derived from aircraft data, *A ric. For. Meteorol.*, *111*, 237–263.

Lin, J. C., and C. Gerbig (2005), Accounting for the effect of transport errors on tracer inversions, *Geophys. Res. Lett.*, *32*, L01802, doi:10.1029/2004GL021127.

Lloyd, J., et al. (2001), Vertical profiles, boundary layer budgets, and regional flux estimates for CO_2 and its $^{13}C/^{12}C$ ratio and for water vapor above a forest/bog mosaic in central Siberia, *Global Biogeochem. Cycles*, *15*(2), 267–284.

Nicholls, M. E., A. Scott Denning, L. Prihodko, P.-L. Vidale, I. Baker, K. Davis, and P. Bakwin (2004), A multiple scale simulation of variations in atmospheric carbon dioxide using a coupled biosphere-atmosphere model, *J. Geophys. Res.*, *109*, D18117, doi:10.1029/2003JD004482.

Perez-Landa, G., P. Ciais, M. J. Sanz, B. Gioli, F. Miglietta, J. L. Palau, G. Gangoiti, and M. M. Millan (2006a), Mesoscale circulations over complex terrain in the Valencia coastal region, Spain, Part 1: Simulation of diurnal circulation regimes, *Atmos. Chem. Phys. Disc.*, *6*, 2809–2852. (Available at http://www.atmos-chem-phys-discuss.net/6/2809/2006/)

Perez-Landa, G., P. Ciais, G. Gangoiti, J. L. Palau, A. Carrara, B. Gioli, F. Miglietta, M. Schumacher, M. M. Millan, and M. J. Sanz (2006b), Mesoscale circulations over complex terrain in the Valencia coastal region, Spain, part 2: Linking CO_2 surface fluxes with observed concentrations, *Atmos. Chem. Phys. Disc.*, *6*, 2853–2895. (Available at http://www.atmos-chem-phys-discuss.net/6/2853/2006/)

Pielke, R. A., and M. Uliasz (1998), Use of meteorological models as input to regional and meso-scale air quality models–Limitations and strengths, *Atmos. Environ.*, *32*(8), 1455–1466.

Pielke, R. A., W. R. Cotton, R. L. Walko, C. J. Tremback, M. E. Nicholls, M. D. Moran, D. A. Wesley, T. J. Lee, and J. H. Copeland (1992), A comprehensive meteorological modeling system–RAMS, *Meteorol. Atmos. Phys.*, *49*, 69–91.

Pielke, R. A., R. L. Walko, L. T. Steyaert, P. L. Vidale, G. E. Liston, W. A. Lyons, and T. N. Chase (1999), The influence of anthropogenic landscape changes on weather in South Florida, *Mon. Weather Rev.*, *127*, 1663–1673.

Prentice, I. C., G. D. Farquhar, M. J. R. Fasham, M. L. Goulden, M. Heimann, V. J. Jaramillo, H. S. Khehgi, C. Le Quéré, R. J. Scholes, and D. W. R. Wallace (2001), The carbon cycle, and atmospheric carbon dioxide, in C*limate Change 2001: The Scientific Basis. Contribution of Working Group I to the Third Assessment Report of the Intergovernmental Panel on Climate Change*, edited by J. T. Houghton et al., pp. 183–237, Cambridge Univ. Press, New York.

Reichstein, M., J. D. Tenhunen, O. Roupsard, J.-M. Ourcival, S. Rambal, F. Miglietta, A. Peressotti, M. Pecchiari, G. Tirone, and R. Valentini (2002), Severe drought effects on ecosystem CO_2 and H_2O fluxes at three Mediterranean evergreen sites: Revision of current hypotheses?, *Global Change Biol.*, *8*, 999–1017.

Rödenbeck, C., S. Houweling, M. Gloor, and M. Heimann (2003), CO_2 flux history 1982–2001 inferred from atmospheric data using a global inversion of atmospheric transport, *Atmos. Chem. Phys.*, *3*, 1919–1964.

Schmitgen, S., H. Geiss, P. Ciais, B. Neininger, Y. Brunet, M. Reichstein, D. Kley, and A. Volz-Thomas (2004), Carbon dioxide uptake of a forested region in southwest France derived from airborne CO_2 and CO measurements in a quasi-Lagrangian experiment, *J. Geophys. Res.*, *109*, D14302, doi:10.1029/2003JD004335.

Schulze, E.-D., et al. (1999), Productivity of forests in the Eurosiberian boreal region and their potential to act as a carbon sink–A synthesis, *Global Change Biol.*, *5*, 703–722.

Schumacher, M. (2005), Airborne and ground level flask sampling for regional carbon budgets–The potential of multiple tracer and isotope analyses. Development of a new 'Investigation Strategy' and of an improved 'Sampling System', Ph.D. thesis, Univ. of Hamburg, Hamburg, Germany.

Shibistova, O., J. Lloyd, S. Evgrafova, N. Savushkina, G. Zraszevskaya, A. Arneth, A. Knohl, O. Kolle, and E.-D. Schulze (2002), Seasonal and special variability in soil CO_2 efflux rates for a central Siberian *Pinus sylvestris* forest, *Tellus, Ser. B*, *54*, 552–567.

Styles, J., M. J. Lloyd, D. Zolotoukhine, K. A. Lawton, N. M. Tchebakova, R. J. Francey, A. Arneth, D. Salamakho, O. Kolle, and E.-D. Schulze (2002), Estimates of regional surface carbon dioxide exchange and carbon and oxygen isotope discrimination during photosynthesis from concentration profiles in the atmospheric boundary layer, *Tellus, Ser. B*, *54*, 768–783.

Tans, P., I. Fung, and T. Takahashi (1990), Observational constraints on the global atmospheric CO_2 budget, *Science*, *247*, 1431–1438.

Tchebakova, N. M., O. Kolle, D. Zolotoukhine, A. Arneth, J. M. Styles, N. N. Vygodskaya, E.-D. Schulze, O. Shibistova, and J. Lloyd (2002), Inter-annual and seasonal variation of energy and water vapour fluxes above *Pinus sylvestris* forest in the Siberian middle taiga, *Tellus, Ser. B*, *54*, 537–551.

Valentini, R., et al. (2000a), Respiration as the main determinant of carbon balance in European forests, *Nature*, *404*, 861–865.

Valentini, R., S. Dore, G. Marchi, D. Mollicone, M. Panfyorov, C. Rebmann, O. Kolle, and E.-D. Schulze (2000b), Carbon and water exchange of two contrasting central Siberian landscape types: Regenerating forest and bog, *Functional Ecol.*, *14*, 87–96.

van der Molen, M. K., A. J. Dolman, M. J. Waterloo, and L. A. Bruijnzeel (2006), Climate is affected more by maritime than by continental land use change: A multiple scale analysis, *Global Planet. Change*, *54*(1–2), 128–149.

Wieringa, J. (1986), Roughness dependent geographical interpolation of surface wind speed averages, *Q. J. R. Meteorol. Soc.*, *112*, 867–889.

Wilson, K. B., et al. (2002a), Energy partitioning between latent and sensible heat flux during the warm season at FLUXNET sites, *Water Resour. Res.*, *38*(12), 1294, doi:10.1029/2001WR000989.

Wilson, K. B., et al. (2002b), Energy balance closure at FLUXNET sites, *Agric. For. Meteorol.*, *113*(1–4), 223–243.

Wilson, K. B., et al. (2003), Diurnal centroid of ecosystem energy and carbon fluxes at FLUXNET sites, *J. Geophys. Res.*, *108*(D21), 4664, doi:10.1029/2001JD001349.

Wirth, C., et al. (1999), Above-ground biomass and structure of pristine Siberian Scots pine forests as controlled by competition and fire, *Oecologia*, *121*, 66–80.

Xian, Z., and R. A. Pielke (1991), The effects of width of landmasses on the development of sea breezes, *J. Appl. Meteorol.*, *30*, 1280–1304.

A. J. Dolman and M. K. van der Molen, Department of Hydrology and Geo-Environmental Sciences, Faculty of Earth and Life Sciences, Vrije Universiteit Amsterdam, De Boelelaan 1085, NL-1081 HV Amsterdam, Netherlands. (han.dolman@falw.vu.nl; michiel.van.der.molen@falw.vu.nl)